Time-resolved monitoring of composite Nafion™ XL membrane degradation induced by Fenton's reaction

Mylène Robert, Assma El Kaddouri, Jean-Christophe Perrin, Jésus Raya, Olivier Lottin

Time-resolved monitoring of composite Nafion™ XL membrane degradation induced by Fenton's reaction

Mylène Robert, Assma El Kaddouri, Jean-Christophe Perrin, Jésus Raya, Olivier Lottin

PII: S0376-7388(20)31550-7

DOI: https://doi.org/10.1016/j.memsci.2020.118977

Reference: MEMSCI 118977

To appear in: *Journal of Membrane Science*

Received Date: 15 October 2020

Revised Date: 7 December 2020

Accepted Date: 9 December 2020

Please cite this article as: Mylè. Robert, A. El Kaddouri, J.-C. Perrin, Jé. Raya, O. Lottin, Time-resolved monitoring of composite Nafion™ XL membrane degradation induced by Fenton's reaction, *Journal of Membrane Science* (2021), doi: https://doi.org/10.1016/j.memsci.2020.118977.

Mylène Robert: Conceptualization, Methodology, Validation, Investigation, Data Curation, Visualization, Writing - Original Draft, Writing - Review & Editing. **Assma El Kaddouri**: Conceptualization, Methodology, Visualization, Supervision, Writing - Original Draft, Writing - Review & Editing. **Jean-Christophe Perrin**: Conceptualization, Methodology, Supervision, Writing - Original Draft, Writing - Review & Editing. **Jésus Raya**: Resources, Methodology, Validation. **Olivier Lottin**: Project Administration, Conceptualization, Methodology, Writing - Original Draft, Writing - Review & Editing.

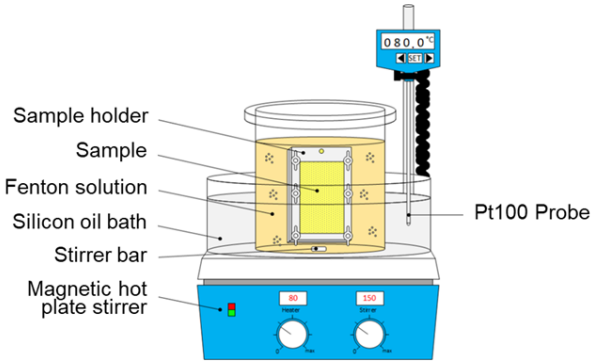

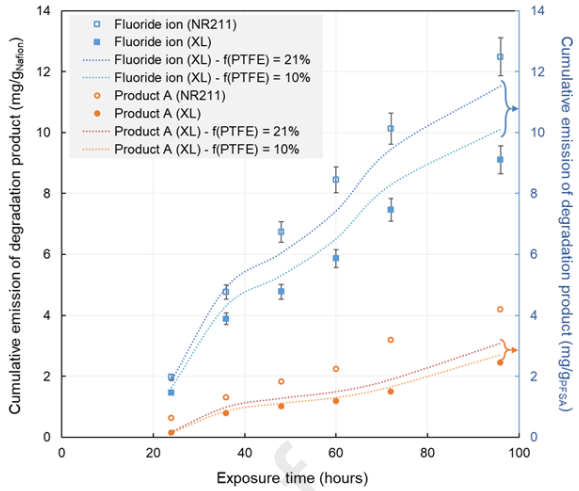

Time-resolved monitoring of composite Nafion™ XL membrane degradation induced by Fenton's reaction

Mylène Robert[a,*], Assma El Kaddouri[a], Jean-Christophe Perrin[a], Jésus Raya[b], Olivier Lottin[a]

[a] *Université de Lorraine, CNRS, LEMTA, F-54000 Nancy, France*

[b] *Membrane Biophysics and NMR, Institut de Chimie de Strasbourg (ICS), UMR 7177 CNRS, Université de Strasbourg, Strasbourg*

[*] *Corresponding author.*

E-mail addresses: mylene.robert@univ-lorraine.fr (M. Robert), assma.el-kaddouri@univ-lorraine.fr (A. El Kaddouri), jean-christophe.perrin@univ-lorraine.fr (J.-C. Perrin), olivier.lottin@univ-lorraine.fr (O. Lottin).

Abstract

Although proton-exchange membrane fuel cells (PEMFC) are considered as a safe and clean energy technology, ageing phenomena of the membrane-electrode assembly (MEA), and more particularly of the membrane, still restrict PEMFC lifetime. In this paper, *ex-situ* accelerated chemical degradation – *via* Fenton's reagents exposure – of reinforced Nafion™ XL membrane is performed in order to investigate the impact of chemical degradation on membrane structure and properties in comparison with unreinforced Nafion™ NR211 membrane. Results demonstrated that both XL and NR211 membranes undergo chemical decomposition after exposure to Fenton's reagents at different degradation rate. Emissions of two main degradation products released by the Nafion™ membranes were monitored as a function of exposure time, demonstrating the greater stability of the XL membrane compared to the NR211 membrane. However, the impact of chemical degradation on water sorption and water transport properties seems negligible for both membranes. This study aims at providing new insight on chemical degradation of composite Nafion™ XL membrane.

Keywords

Chemical degradation; Durability; Fenton's reaction; Nafion™ XL membrane; PEM fuel cell

1. Introduction

Proton-exchange membrane fuel cell (PEMFC) is a promising technology for replacing fossil energies in stationary and transportation applications. In spite of numerous key technological advances over the past decades, their large-scale commercialization is still impeded by durability and performance issues [1–3]. Perfluorosulfonic acid (PFSA) membranes are today the most-commonly used materials in PEMFC systems thanks to their remarkable proton conductivity and their chemical-mechanical stability, despite an excessively high degradation rate during fuel cell operation [4].

In recent years, countless studies have been carried out to provide key information on the degradation mechanisms of PFSA membranes and the impact on their structure and properties. The degradations are due to chemical and mechanical stresses generated during fuel cell operation. They may go unnoticed for thousands of hours of operation, as membrane thinning does not always lead to a decrease in performances, but they will eventually be at the origin of critical failures when the membrane breaks [5,6].

Chemical degradation results from the formation of hydrogen peroxide, permitted by the crossover of reactant gases through the membrane, which then decomposes to form highly reactive oxygen species (ROS): the hydroxyl ($HO^{\bullet}$), hydroperoxyl ($HOO^{\bullet}$) and hydrogen ($H^{\bullet}$) radicals [7–9]. These reactive oxygen species attack the most vulnerable bonds of the PFSA structure, located both in the fluorocarbon backbone and the perfluorinated side chains [8], leading to a loss of membrane integrity and consequently to its thinning [10,11]. In the case of the first generations of Nafion™ membranes, the carboxylic acid end groups, introduced during the manufacturing process, were the main sites where degradation began. Membranes of the current generation are chemically stabilized thanks to an additional step of post-

fluorination [12] and have a better durability. In addition to chemical degradation, the durability of the membrane is also significantly altered by a mechanical fatigue, mainly due to numerous swelling/shrinkage cycles and to the non-uniform distribution of the contact pressure with the flow field plates [13]. This fatigue leads to the formation and growth of creeps, cracks and pinholes [14–17]. It is now well established that chemical and mechanical stresses interact with each other leading to an acceleration of the overall degradation rate [18–21].

To fully understand their impact on the properties of PFSA membranes, it is advisable to study chemical and mechanical stressors separately, but also together. In that respect, specific accelerated stress tests (AST) mimicking chemical and/or mechanical stresses have been developed with both *in-situ* and *ex-situ* approaches [21–23]. Among them, Fenton's reaction is the most widely used *ex-situ* degradation protocol for reproducing the aggressive chemical environment and especially the formation of free radicals encountered during fuel cell operation. Fenton's reaction consists in the reaction between hydrogen peroxide and iron ions to form hydroxyl and hydroperoxyl radicals according to the following equations (1-3):

$$H_2O_2 + Fe^{2+} \rightarrow Fe^{3+} + HO^{\bullet} + HO^{-} \quad (1)$$

$$H_2O_2 + HO^{\bullet} \rightarrow HOO^{\bullet} + H_2O \quad (2)$$

$$HOO^{\bullet} + Fe^{3+} \rightarrow Fe^{2+} + H^{+} + O_2 \quad (3)$$

Healy *et al.* investigated the degradation of Nafion™ membranes through *in-situ* (fuel cell operation) and *ex-situ* (Fenton's reaction) experiments and demonstrated by ^{19}F-NMR spectroscopy that similar fluorocarboned molecules deriving from the PFSA side-chain were released in both cases [11]. The usual indicators of chemical degradation are the emissions of fluoride ions [11,12,24–28], a drop of proton conductivity [28–31] and a decrease of the ion-exchange capacity (IEC) [28,30,31]. Some authors have also monitored the evolution of the chemical structure of PFSA by Fourier-transform infrared (FTIR) spectroscopy and reported a

decrease of the typical vibration bands of PFSA structure [24,27,28,32]. Other authors, however, did not detect any significant evolution of the infrared spectra [25,33]. Recently, Luo *et al.* [31] studied the effect of chemical degradation on water transport properties of PFSA membranes and revealed the existence of a strong correlation between the water permeability of the membrane and the exposure time to Fenton's reagents. They observed important physical defects and a significant increase of water uptake resulting in larger hydrophilic volume fraction and higher proton mobility.

Through the years, several strategies have been developed to overcome PFSA membranes durability and performance issues: in particular, reinforced composite membranes containing a thin microporous polytetrafluoroethylene (PTFE) layer have been developed by W. L. Gore & Associates, Inc. (Gore-SELECT®) and by Dupont de Nemours, Inc. (Nafion™ XL) allowing the use of thinner membranes with similar proton conductivity than unreinforced ones. Composite membranes indeed demonstrate an extended lifetime during fuel cell operation [23] thanks to a better dimensional and mechanical stability [34], an increased resistance to crack initiation and propagation [17,35], as well as a higher resistance [36,37]. In addition, XL membranes are more enduring against chemical degradation thanks to the introduction of cerium-based radical scavengers [38–40]. In recent years, the Ce^{3+}/Ce^{4+} couple has become a promising candidate to efficiently neutralize radicals and protect ionic groups thanks to its self-regenerative property. However, despite the presence of mechanical reinforcements and radical scavengers, current membranes are still insufficiently durable during fuel cell operation [16,41].

In the past decades, most of the studies investigated the chemical degradation of the first (N112-N115-N117) and second (NR211-NR212) generations of Nafion™ membranes whereas only a few were focused on the reinforced Nafion™ XL membrane [17,35,41,42]. In this work, the chemical degradation of Nafion™ XL membrane is monitored as a function of the

exposure time to Fenton reagents using several indicators such as the fluoride emissions or the evolution of the chemical structure observed by FTIR spectroscopy. The results are compared with those of its non-reinforced analogue, the Nafion™ NR211 membrane. After 96 hours of exposure, the membranes were characterized using a series of techniques (DVS Analyzer, ^{1}H-NMR) in order to clarify the contribution of the reinforcement against the chemical degradation.

2. Experimental

2.1 Materials and preparation

Nafion™ XL & NR211 membranes were purchased from Ion Power Inc. in the protonated form (H^{+}). These PFSA membranes have similar chemical composition since they are obtained by the copolymerization of perfluoro(4-methyl-3,6-dioxa-7-octene-1-sulfonyl fluoride) and tetrafluoroethylene (TFE) [43]. They also have similar Ion Exchange Capacity (IEC) of 0.92 meq.g^{-1} for XL and 0.98 meq.g^{-1} for NR211 and nominal thicknesses – 27.5 µm for XL and 25.4 µm for NR211. Compared to Nafion™ NR211, Nafion™ XL has an additional reinforcement based on a microporous matrix rich in PTFE and contains radical scavengers based on cerium species [38].

The commercial membrane samples were pretreated before any use following a specific procedure similar to the one established by Xu *et al.* [44]: they were first boiled one hour in a 3 wt.% hydrogen peroxide solution and rinsed thoroughly with distilled water in order to eliminate any organic impurities. They were then soaked 30 minutes at room temperature in a solution of nitric acid (10 mol.L^{-1}) and boiled one hour in deionized water. The samples were then boiled one hour in a sulfuric acid solution (1 mol.L^{-1}), and one hour again in deionized water to ensure a complete substitution of the ionomer active sites. Finally, they were dried 24 hours in an oven at 60°C.

120 *2.2 Ex-situ Fenton's test*

121 The chemical degradation protocol is based on the Fenton's reaction [45] and consists in the
122 reaction between ferrous ion (Fe^{2+}) and hydrogen peroxide (H_2O_2) to form hydroxyl ($HO^{\bullet}$)
123 and hydroperoxyl ($HOO^{\bullet}$) radicals. The concentration of Fenton's reagents was established
124 upon previous studies [46,47]. A stock solution containing 50 $mg.L^{-1}$ of ferrous ions was first
125 prepared from iron (II) sulfate heptahydrate ($FeSO_4.7H_2O$) provided by Jeulin. A few drops of
126 concentrated nitric acid were then added to lower the pH below 3 before the addition of
127 hydrogen peroxide. Finally, the 50 $mg.L^{-1}$ stock solution was mixed with 30 vol.% hydrogen
128 peroxide (VWR Chemicals) to produce a solution containing 3 vol.% of hydrogen peroxide
129 and 1 ppm of ferrous ion.

130 Pieces of membranes (6 cm x 4 cm) were fixed in a sample holder to ensure proper surface
131 flatness and uniform exposure of the membrane to the solution. 250 cm^3 of the Fenton
132 solution containing 1 ppm of Fe^{2+} and 3 vol.% of H_2O_2 was poured into a dry beaker placed in
133 a silicon oil bath at 80°C under magnetic stirring. The membrane was fully immersed in the
134 Fenton's solution for several hours and a watch glass was put at the top of the beaker to
135 minimize the evaporation (a schematic representation of the setup can be seen figure 1 of
136 reference [47]). The experiment lasted 24, 36, 48, 60, 72 and 96 hours and fresh solutions
137 were thus prepared and used at times 0, 24, 36, 48, 60 and 72 hours. Fluoride ions having a
138 great affinity for silica-based materials, the depleted Fenton solutions were stored in
139 polyethylene vessels for further analyses after each renewal. The membranes samples were
140 then treated so that they can be analyzed by FTIR spectroscopy. In order to eliminate cationic
141 contaminant due to iron ions, the samples were thoroughly rinsed with distilled water before
142 being soaked in a complexing solution of ethylenediaminetetraacetic acid disodium (EDTA-
143 Na_2 – 0.01 $mol.L^{-1}$) at room temperature overnight. They were then boiled in a nitric acid
144 solution (HNO_3 – 1 $mol.L^{-1}$) at 80°C during two hours for re-acidification and washed two

hours in distilled water at 80°C. Finally, the membrane samples were dried approximately 20 hours in an oven at 60°C before FTIR analysis. After that, they were put back into a fresh Fenton solution to pursue the chemical degradation process.

2.3 Release of fluoride ions

After each renewal of the Fenton solution, the concentration of the fluoride ions released by the membranes was evaluated with a pH/millivolt meter (SevenCompact S220, Mettler Toledo) equipped with a fluoride ion-selective electrode (DX219, Mettler Toledo). Prior to the measurement, the electrode was calibrated over the range 0.057 – 19 ppm using specific diluted solutions prepared from 1000 ppm standard solution (Mettler Toledo). 25 mL of TISAB II solution were added to 25 mL of sample solution to stabilize the ionic force of the analyzed species. The detection limit of the electrode provided by the supplier is of about 0.01 ppm.

2.4 FTIR-ATR spectroscopy

Infrared spectra were obtained using a FTIR spectrometer (Vertex 80v, Bruker) equipped with a DTGS detector, a KBr beam splitter and a single reflection diamond ATR accessory. The spectra were recorded at room temperature with accumulation of 16 scans and a wavenumber resolution of 1 cm^{-1} from 400 to 6000 cm^{-1} in absorption mode. Prior to each analysis, the membrane samples were exposed to a dry nitrogen flow (99.9999 % of purity) with a 1 NL/min flow rate during 10 minutes in order to dry the membrane and perform analysis in the same conditions for all measurements and samples. The measurements were performed at various locations on the surface of the membrane samples and on both sides in order to check the homogeneity of the chemical structure for pristine membranes and to investigate aging heterogeneities in the case of the aged samples.

2.5 Dynamic Vapor Sorption

The water sorption isotherms were measured using an IGASorp (Hidden Isochema, UK) dynamic vapor sorption (DVS) analyzer with a mass resolution of ±1 µg. The samples were first dried five hours under dry nitrogen at a temperature of 60°C to reach nearly 0 % RH and thus set the dry mass, even though it has been demonstrated that some "residual water" still remains in the membrane even after drastic drying protocols [48,49]. The sorption isotherms were then recorded at 30 ± 0.1°C for a water activity varying between 0.05 and 0.95, with an increment of 0.05. The equilibrium threshold was fixed to 99 % and the equilibration time of each step ranged between 3 and 10 hours.

2.6 NMR Spectroscopy

2.6.1 Solid-state ^{19}F-NMR

Solid-state ^{19}F-NMR experiments were performed at 470.5 MHz on a Bruker Avance 500 wide-bore spectrometer equipped with a H/F/X magic-angle spinning (MAS) probe. The samples were rolled and loaded into 2.5 mm zirconia thin walls rotors with Vespel bottom and drive caps. All spectra were measured with a Hahn-echo pulse sequence at 24°C under MAS conditions with a frequency spinning of 25 kHz. Each experiment was performed with the following parameters: a 90° pulse width of 1.25 µs, a recycle delay of 10 s, a dwell time of 2.5 µs and a number of accumulations of 64 scans.

2.6.2 Liquid state ^{19}F-NMR

Prior to the NMR analysis the remaining Fenton solutions to which the XL and NR211 membranes were exposed were concentrated using a rotary evaporator (Rotavapor R-100, Büchi) in order to evaporate the maximum amount of water (the initial volume of solution was decreased by a factor of ten). This step was essential to improve the quality of the signal and decrease the acquisition time. Samples of concentrated Fenton solution were poured into 5 mm NMR tubes and mixed with deuterium oxide (D_2O) for a final D_2O/H_2O ratio of 20:80.

The experiments were conducted on a Bruker Avance III 400 spectrometer operating at the Larmor frequency of 376.5 MHz and using a 5 mm BBFO probe. Both qualitative and quantitative NMR experiments were performed in this study. The qualitative experiments were carried out at room temperature with the following parameters: a 90° pulse width of 13.5 µs, a spectral width of 200 ppm, a recycle delay of 1 s and an acquisition time of 0.87 s. The ^{19}F-NMR spectra were obtained thanks to conventional single pulse experiments with a number of accumulations between 2048 and 30720.

Quantification by ^{19}F-NMR was based on a protocol recently established by El Kaddouri *et al.* [50]. The objective of the work was to propose a new and efficient ^{19}F-NMR quantification protocol able to measure the concentration of fluorinated molecules in PFSA solutions. The first step consists in estimating the order of magnitude of the fluorine concentration using the signal to noise ratio, which is conventionally defined as the ratio between a resonance peak height and the noise amplitude. The second step is to use an external reference whose fluorine concentration lies in the range determined in the first step. This two-step method was essential for our study due to the low concentration of decomposition products in the Fenton solutions. Following this quantification protocol, the concentration of the decomposition products was first estimated by measuring the (S/N) ratio using the "SINO function" integrated into the TopSpin 3.5 software. The use of an external reference of trifluoroethylene (TFT) solution with an appropriate concentration permitted then to determine more accurately the fluorine concentration. The TFT solution was placed in a coaxial insert inside the NMR tube.

The experiments were performed at 300K with a 90° pulse width of 13.5 µs, a spectral width of 200 ppm, and a number of accumulations between 12000 and 16384. For accurate quantitative NMR experiments, the recycle delay should be higher than five times the relaxation time T_1 of the target molecule. The relaxation time of Nafion™ ionomer solutions

was determined by Yuan *et al.* [51] to be 0.92 ± 0.05 s and that of TFT was determined by El Kaddouri *et al.* [50] to be 1.5 ± 0.1 s. Consequently, the recycle delay was fixed to 8 s for all quantitative NMR experiments.

2.6.3 Liquid state ^{1}H-NMR

The experiments were performed on a Bruker Avance III 600 WB spectrometer with a Larmor frequency of 600.13 MHz equipped with a 5 mm Diff30 probe capable of delivering a gradient intensity up to 1800 G.cm^{-1}. The spectra were recorded at room temperature by accumulating 256 scans and using a recycle delay of 3 s and a dwell time of 25 µs. An optimization of the proton 90° pulse width P1 was carried out for each sample before recording the spectra. A Pulsed-Gradient STimulated spin-Echo (PGSTE) sequence with unipolar gradients was used to measure the water self-diffusion coefficients. The measurements were performed with the following parameters: a gradient pulse duration δ = 0.66 – 1.50 ms, a diffusion delay Δ = 6.78 – 10.00 ms and a gradient strength g = 40 – 1 000 G.cm^{-1}. The water self-diffusion coefficient was then calculated by fitting the observed signal attenuation against the magnitude of the applied gradient strength g using the Stejskal – Tanner equation [52].

Pulsed Field Gradient (PFG) NMR is a common and accurate method for measuring the water diffusion coefficient in Nafion™ membranes [53]. The water self-diffusion coefficient in pristine and aged membrane samples were here determined as a function of the water uptake. For this purpose, each sample (approximately 1 x 5 cm) was first fully immersed in distilled water at room temperature for 3 hours. Once out of the water, the samples were quickly pressed between two layers of absorbent paper in order to remove any residual water droplets from the surface before being rolled and packed into 5 mm airtight NMR tubes. The samples were equilibrated at least overnight before being weighted and analyzed. The hydration level

of each sample was then adjusted by exposing the samples to a water-saturated environment or to the ambient atmosphere, respectively to increase or decrease the water content.

3. Results

3.1 Evolution of the chemical structure after exposure to Fenton's reagents

3.1.1 FTIR-ATR spectroscopy

FTIR spectroscopy was performed with an ATR accessory to study exclusively the surface of the XL membranes and thus exclude its microporous polytetrafluoroethylene (PTFE) central layer from the analysis. Fig. 1a illustrates the infrared spectra of pristine membranes in the range 1400 – 850 cm^{-1} where the characteristic vibration modes of the PFSA are visible. The vibration bands in this range have been assigned in the literature [48,54–57] and five characteristic vibration bands have been outlined as illustrated in Fig. 1a (the spectra are normalized to the most intense band at 1144 cm^{-1} associated to the asymmetric -CF_2 stretching mode). As described in section 2.4, the homogeneity of the chemical structure over the surface was verified by systematically performing at least three local measurements on both sides of the samples (pristine or aged with different exposure time). In this regard, Fig. 1b shows the averaged intensity of the side chain stretching bands as a function of exposure time to Fenton reagents: the intensity of the C–O–C and the S–O stretching bands do not vary significantly over the exposure time, regardless of the type of membrane. The experimental values are given in Table A.1 of the Appendix. Additionally, one can notice on Fig. 3a that the normalized intensity of sulfonate groups at 1160 cm^{-1} varies between a pristine XL membrane and a NR211 one. It is important to note that the XL is a composite membrane constituted by a non-conductive PTFE-rich reinforcement impregnated on both sides with PFSA ionomer. Consequently, the IEC measured for its global structure will differ from that of the 100% PFSA external layers. Indeed, Moukheiber *et al.* demonstrated that the IEC of

external PFSA layers in XL is 1.10 ± 0.03 meq.g^{-1} [58], which is higher than that of NR211 membrane (0.98 ± 0.03 meq.g^{-1}) exclusively composed of PFSA. This difference is thus at the origin of the discrepancy in the normalized intensities of SO_3 vibration band between the membranes [58].

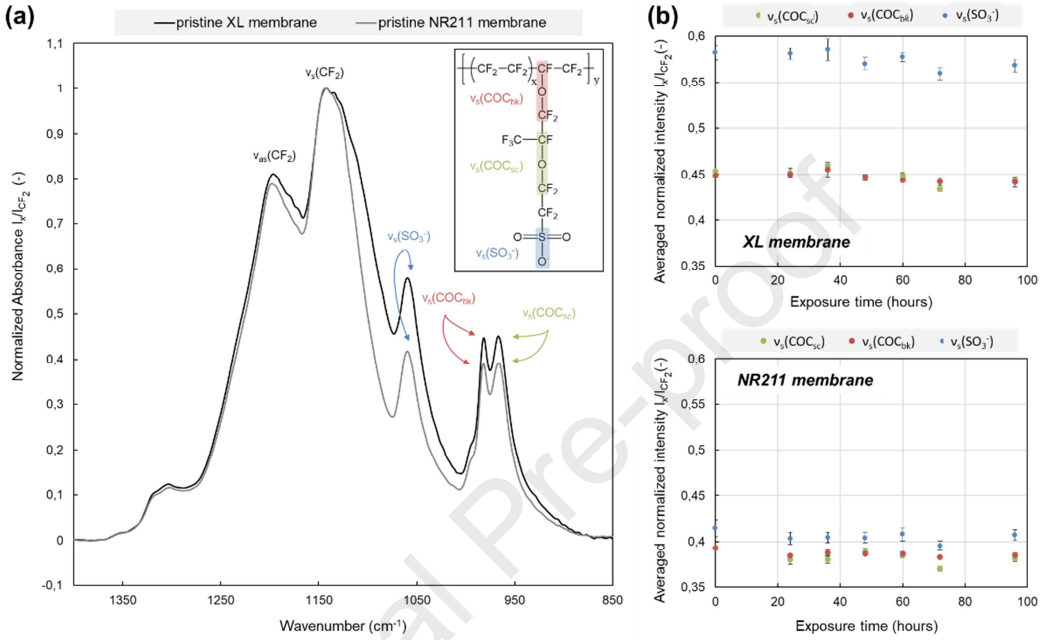

Fig. 1. (a) IR spectra of pristine XL and NR211 membranes focused on PFSA absorption bands and (b) evolution of averaged normalized intensity of the bands associated to the PFSA side chain over exposure time for XL (top right corner) and NR211 (bottom right corner) membranes. The inset in figure 1a illustrates the attribution of PFSA side-chain bands [48,54–57].

The constant intensity ratio between the side chain and the -CF_2 (predominantly in the main chain) vibration bands may result from two distinct behaviors: either there is no significant chemical degradation occurring or the chemical degradation induces both side and main chains decomposition in similar proportion: in this last case, the normalized intensity ratios I_x/I_{CF_2} may not change drastically. It has been shown in the literature that chemical degradation – in both *in-situ* and *ex-situ* conditions – can follow this trend, with possibly an evolution of the chemical structure of Nafion™ membranes that remains non-detectable with FTIR or solid NMR measurements [25,33,59]. For example, Kundu *et al.* reported no apparent change in chemical structure by FTIR as well as no change in IEC after chemical

degradation by Fenton's reaction [25]. Nevertheless, they measured significant fluoride ion emissions and weight losses as well as important morphology evolutions, with the appearance of numerous cracks and bubbles at the membrane surface, evidencing the presence of significant chemical degradation. Furthermore, the constant intensity ratio between $-SO_3^-$ (side chain fragment) and $-CF_2$ (mostly main chain fragment) vibration bands also suggests that the IEC does not evolve after exposure to Fenton's reagents, as confirmed by ^{19}F-NMR spectroscopy in the following.

3.1.2 Solid-state ^{19}F-NMR spectroscopy

Although FTIR-ATR spectroscopy only permits to analyze the ionomer surface (on a few µm depth), it is believed to be quite representative of the overall PFSA structure since the membrane thickness is in the range 25–30 µm and degradations are expected to be homogeneous. Nevertheless, to confirm observations made by FTIR-ATR and to quantify the IEC, the overall chemical structure of degraded XL and NR211 membranes has been analyzed by solid-state ^{19}F-NMR spectroscopy. Fig. 2 illustrates the spectra of pristine and degraded Nafion™ membranes as well as the experimental IEC determined from these spectra. The resonance peaks of Nafion™ have already been identified and assigned in the literature [60–62]. CF_2 groups of the Nafion™ backbone is attributed to the resonance at -118 ppm by analogy with the NMR signal of PTFE while the CF group located at the junction between the backbone and the side chain gives rise to a peak at -135 ppm. The side chains signals appear at -76 ppm for the CF_3 and CF_2 groups close to ether linkages, at -140 ppm and around -113 ppm for the CF and CF_2 groups close to the sulfonic sites, respectively.

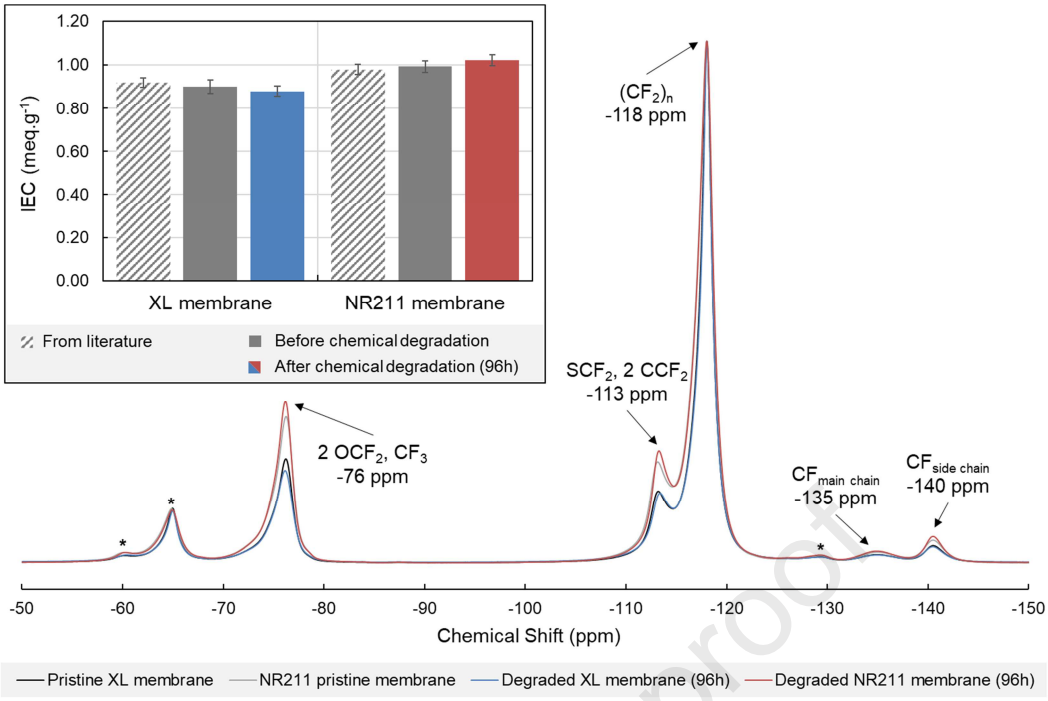

Fig. 2. ^{19}F MAS NMR spectra and resonance peak assignment of Nafion™ XL and NR211 membranes before and after chemical degradation. The resonance peaks with an asterisk designate spinning sidebands. The inset illustrates experimental IEC deduced from spectra in comparison with the literature values [58,63].

As shown in Fig. 2, the intensity of side chain resonance peaks does not significantly vary after 96 hours of Fenton's reagents exposure for both membranes, which supports the observations made by FTIR-ATR.

Furthermore, the integral of each resonance peak – associated to a specific fluorinated fragment of the polymer structure – is proportional to the number of fluorine atoms in this fragment. This makes it possible to evaluate the IEC through a theoretical relationship between the IEC and the ratio of the signal integral at -76 ppm ($I_{-76\ ppm}$), to those at -114 and -118 ppm ($I_{-114\ and-118\ ppm}$). The IEC is related to this ratio through n, the number of moles of tetrafluoroethylene (TFE) per moles of comonomer unit, according to the following equation:

$$IEC = \frac{1000}{EW} = \frac{1000}{100n + M} = \frac{1000}{100 \times \left(\frac{7}{4} \times \frac{I_{-114\ and-118\ ppm}}{I_{-76\ ppm}} - 1\right) + M}$$

where *M* designates the molecular weight of vinyl ether monomer, equals to 444 $g.mol^{-1}$. These peaks were chosen because they are the most intense and best resolved, and the relationship has been validated by previous studies investigating the IEC evolution of Nafion™ membranes by solid-state ^{19}F-NMR spectroscopy [41,58].

For reinforced XL membrane, the IEC determined from the ^{19}F-NMR spectra is impacted by the presence of the PTFE microporous layer. In that respect, this value is denoted as "global IEC" (IEC_g) to distinguish from the value measured in the case of unreinforced PFSA membranes. Although ^{19}F-NMR does not permit to assess directly the IEC of only the PFSA part of composite membranes, the evolution of IEC_g is sufficient to evaluate the effect of chemical degradation since the PTFE microporous layer is believed to have a good chemical stability against radical attacks.

In this work, the IEC of the NR211 and the IEC_g of XL membranes measured before degradation are in good agreement with the supplier datasheet and literature values [58,63]. After 96 hours of exposure, neither the IEC_g of the XL membrane nor the IEC of the NR211 membrane seemed to have changed significantly. This is consistent with the trend observed by FTIR-ATR spectroscopy stating that the main and side chains of Nafion™ membranes decompose in equal proportion. Other indicators are thus needed to confirm the degradation of both membranes.

3.2 Quantification of the chemical degradation

3.2.1 Weight loss and fluoride emissions

Weight loss is often considered as one of the primary indicators of PFSA chemical decomposition. Fig. 3a shows the weight loss of both membranes as a function of time. The loss is significant and seems more pronounced for NR211: after 96 hours of Fenton's reagents exposure, the weight loss is of about 2 % of the initial dry weight for XL membranes and

around 10 % for NR211 (Fig. 3a). The presence of a PTFE reinforcement layer in the XL membrane probably helped to mitigate the weight loss thanks to a better mechanical strength [36,37]. Indeed, NR211 appeared more fragile than XL during the visual inspections carried out before each renewal of the solutions. Finally, it must be noted that an unquantifiable fraction of the weight loss may be due to the numerous disassembly and reassembly of the polycarbonate frames containing the membranes during the post-treatment process. Nonetheless, both membranes being subjected to the same protocol, this is not the only cause of their different behavior.

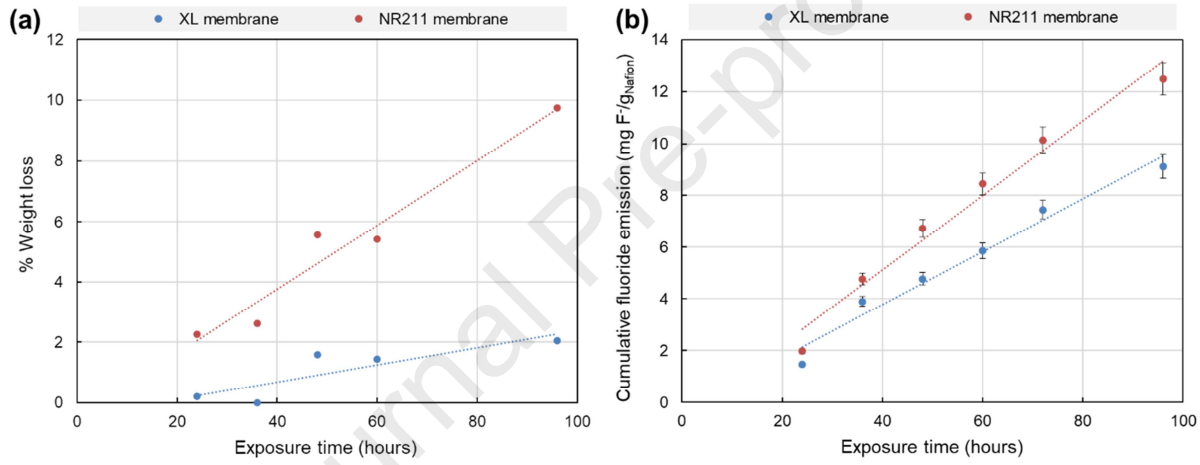

Fig. 3. Evolution of (a) percent weight loss and (b) cumulative fluoride emissions of NR211 and XL membranes as a function of exposure time.

Analysis of Fenton solutions after degradation, as well as the water produced during fuel cell operation, is an efficient way to evaluate the membrane degradation through the detection of degradation products. Among them, fluoride ions, related to the production of hydrofluoric acid (HF) due to radical attacks of the polymer, are believed to be a reliable and ease-to-measure indicator of PFSA decomposition [11,12,19,24–27]. Fig. 3b shows significant and regular fluoride emission rates of about 143.7 $\mu g/g_{Nafion}/h$ for NR211 and 102.4 $\mu g/g_{Nafion}/h$ for XL (*i.e.* after 96 hours: 12.5 mg F^-/g_{Nafion} for NR211 and 9.1 mg F^-/g_{Nafion} for Nafion™ XL). Experimental values of figure 3b are given in Table A.2 in Appendix. Such a tendency

of the emissions to remain quite constant with time has already been highlighted by several authors [12,25,26]. These results clearly demonstrate the effectiveness of the degradation process by Fenton's reaction, even though no chemical structure evolution of the membranes has been put forward. Furthermore, the degraded NR211 membrane seems more impacted than the XL. It is also important to notice that the presence of other molecules in the solution cannot be excluded, as it will be seen in the next section.

3.2.2 Liquid-state ^{19}F-NMR spectroscopy

To pursue the identification and monitoring of the degradation products released by the membranes over exposure time, a deeper investigation of the Fenton solutions was carried out using liquid-state ^{19}F-NMR spectroscopy. Fig. 4 shows the spectra of the Fenton solutions collected between 0 and 24 hours (solution #1), between 24 and 36 hours (solution #2), between 72 and 96 hours (solution #6). They present various sharp resonance peaks corresponding to several fluorinated species. For example, three compounds can be identified in the solution #1 after 24 hours of Fenton's reagents exposure (Fig. 4a):

- The peak at -75.5 ppm is identified as the trifluoroacetic acid (TFA) molecule [64,65],
- The peak at -161 ppm can be attributed to fluoride ions, for which the chemical shift is known to depend on the concentration and/or the counter-ion [66–68],
- A set of resonance peaks, at -80.0 ppm, -80.4 ppm, -82.3 ppm, -82.9 ppm, -83.3 ppm, -118.0 ppm and -126.3 ppm, has been assigned in the literature to the perfluoro(3-oxapentane)-1-sulfonic-4-carboxylic diacid [11,69].

For clarity, the perfluoro(3-oxapentane)-1-sulfonic-4-carboxylic diacid will be thereafter denominated as "product A". It is important to note that some resonance peaks, denoted in Fig. 4 by the symbol (*), are not yet attributed to specific fluorinated compounds. Some unidentified degradation products are therefore present in solution.

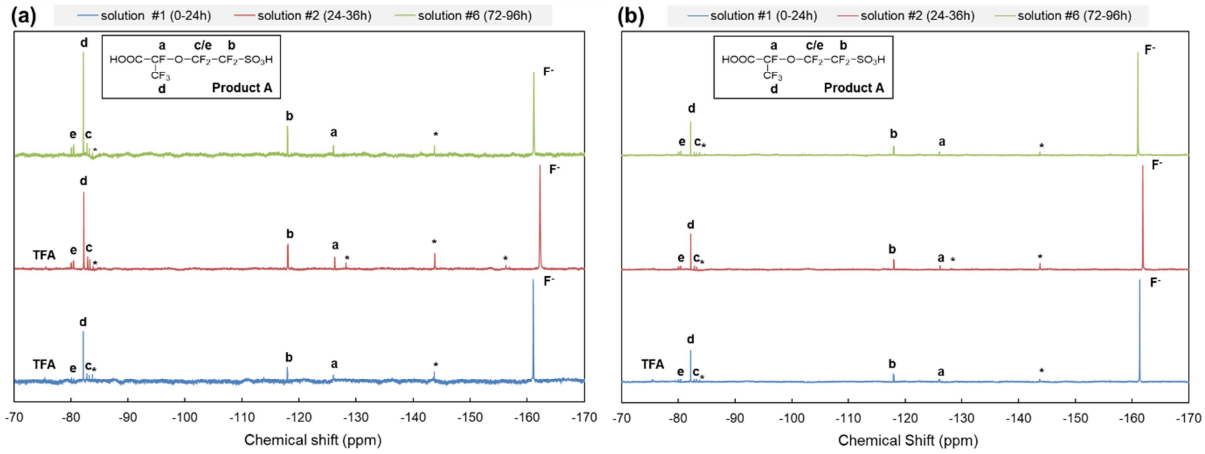

386

387 **Fig. 4.** ^{19}F-NMR spectra of (a) XL membranes and (b) NR211 membranes after 24, 36 and 96 hours of exposure
388 to Fenton's reagents. The inset illustrates the chemical structure of product A and the attribution of its resonance
389 peaks. The resonance peaks with an asterisk designate unidentified molecules.

390 In the literature, analyses of water effluents during fuel cell operation as well as Fenton
391 solutions after *ex-situ* degradation permitted to clearly identify the product A [11,69–71] and
392 the trifluoroacetic acid (TFA) [71,72] as degradation products of PFSA membranes. More
393 particularly, product A has a chemical structure deriving from that of the PFSA side-chain.
394 This compound has also been identified as the main degradation product of PFSA membranes
395 in both *in-situ* (fuel cell operation) and *ex-situ* (Fenton's reaction) aging experiments,
396 demonstrating that the *ex-situ* degradation *via* the Fenton's reaction replicates at least some of
397 the mechanisms involved in fuel cell operation [11]. Furthermore, product A is released by
398 both XL and NR211 membranes all along the degradation process which suggests that the
399 degradation mechanism is similar whether the membrane is reinforced or not and that the
400 mechanism seems to remain unchanged throughout the testing period.

401 Similarly to fluoride ions, the emissions of product A and TFA have been monitored over
402 time thanks to quantitative NMR measurements. The concentrations of product A and TFA
403 were measured after each solution renewal and compared to that of fluoride ions in Fig. 5.
404 Although the quantification of fluoride emissions is also possible by ^{19}F-NMR spectroscopy,
405 measurements *via* the ion-selective electrode is more accurate since NMR measurements

406 required the evaporation of water solvent in Fenton solutions, a step during which molecules
407 having a boiling temperature as low as hydrofluoric acid (19.5°C) may easily evaporate too.
408 Indeed, the analysis of Fenton solutions before and after the evaporation step have been
409 carried out and confirmed that fluoride ions concentrations determined by quantitative NMR
410 are significantly lower than those measured *via* the ion-selective electrode.

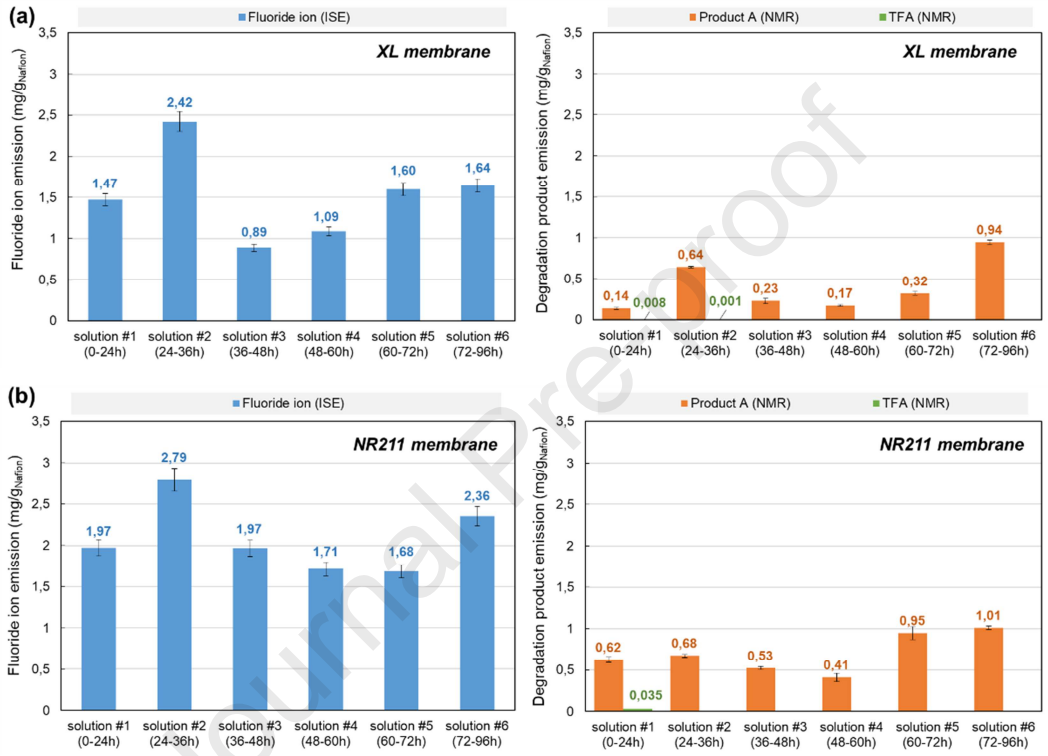

411

412 **Fig. 5.** Evolution of the emissions of the degradation products as a function of exposure time for (a) XL and (b)
413 NR211 membranes. The fluoride emissions were evaluated thanks to the ion-selective electrode while the
414 emissions of Product A and TFA were estimated by NMR.

415 Although the emissions of both fluoride and product A vary during the whole testing period,
416 degradation products are released in the same order of magnitude for both membranes. It can
417 be also noted that degradation product emissions seem slightly higher for NR211 than XL
418 membrane.

419 *3.2.3 Correlation between weight loss and emissions of degradation products*

Table 1 summarizes the total amounts of degradation products emitted in solution in comparison with the weight loss. In the case of the XL membrane, the sum of the emissions reveals that 11.89 mg of degradation products per gram of dry Nafion have been released during the process. This accounts for about 56 wt.% of the global 20.6 mg/g_{Nafion} weight loss. In the case of NR211, a total amount of 17.11 mg of degradation products per gram of dry Nafion have been detected, which only represents 15 wt.% of the total weight loss. As mentioned earlier, an unknown but significant fraction of the weight loss may be due to the multiple disassembly/reassemblies involved in the degradation protocol, more specifically in the case of the unreinforced NR211 membrane.

Table 1 – Weight loss analysis of PFSA membranes after 96 hours of chemical degradation.

	Material loss (mg/g_{Nafion})	Fluoride ion (mg/g_{Nafion})	Product A (mg/g_{Nafion})	TFA (mg/g_{Nafion})
XL membrane	20.60	9.10	2.44	0.01
NR211 membrane	108.30	12.48	4.20	0.04

Moreover, some degradation products were not identified (see section 3.2.2 and Fig. 4) and/or may have evaporated during the degradation process, the system being not perfectly sealed. One must note that fluoride ions, which are present as hydrofluoric acid in acidic media, as well as other small molecules like TFA (its boiling temperature being 72°C) could evaporate upon degradation process taking place at 80°C. Finally, non-fluorinated molecules such as sulfate SO_4^{2-} or hydrogen sulfate HSO_4^- ions can also be released by the membranes in solution during the degradation process [11,29,32,71,72].

3.3 Impact of the degradation on the functional properties of the membranes

3.3.1 Water sorption capacity in degraded membranes

The water sorption property of PFSA membranes is strongly related to their microstructure and ion-exchange capacity (IEC). The sigmoidal shape of the sorption isotherm is a result of

441 the specific two-phase separated morphology of the membrane in which hydrophilic sulfonic
442 sites, hydrophobic phase and water molecules coexist. Water sorption in Nafion™ is generally
443 associated to three distinct sorption mechanisms: the dissociation of the sulfonic groups at
444 low water activity a_w, the adsorption of water molecules and the growth of hydrophilic
445 domains for intermediate hydration levels and the aggregation of water molecules with a
446 bulk-like behavior at high water activities. The first adsorption mechanism, described by the
447 Langmuir adsorption model, characterizes the formation of the solvation shell where sulfonic
448 groups form strong hydrogen bonds with water molecules. For intermediate hydration levels,
449 the adsorbed water molecules are tightly bonded to the initial hydration shell and the
450 mechanism is controlled by Henry's law: this step characterizes the solubility of water within
451 the polymer phase. Finally, the weakly bonded water molecules aggregate when the water
452 activity increases, which entails a macroscopic swelling of the membrane in accordance with
453 its mechanical properties. This swelling conducts to the growth of the hydrophilic domains
454 and their interconnection to form a percolated network of water. In this respect, contribution
455 of Langmuir (C_L) and Henry's (C_H) sorption mechanisms were obtained by fitting
456 experimental data for water activities a_w between 0 and 0.6 according to the following
457 equation:

$$\frac{\Delta m}{m} = C_L + C_H = \frac{A * B * a_w}{1 + B * a_w} + C * a_w$$

458 where $\frac{\Delta m}{m}$ designates the water uptake (wt.%), *A* and *B* are two parameters describing the
459 Langmuir sorption mode and *C* is the Henry's solubility constant. The Cluster sorption
460 contribution is then deduced by subtracting the Langmuir and Henry's contributions from the
461 experimental data.

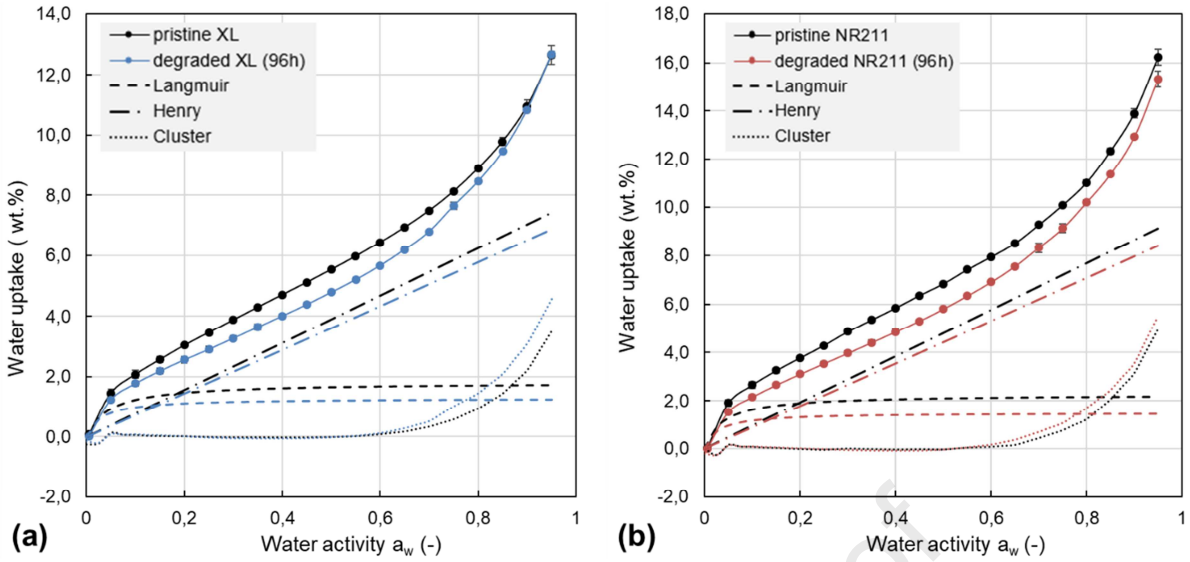

462

463 **Fig. 6 –** Water sorption isotherms (30°C) decomposed into three adsorption mechanisms of (a) XL and (b)
464 NR211 membranes after 96 hours of Fenton's reagents exposure in comparison with pristine membranes. Five
465 measurements were performed on the pristine XL in order to control the repeatability of the measurements and
466 of the pretreatment process. In the case of the degraded membranes, the initial samples were cut into two pieces
467 and the results of the two measurements were averaged.

468 Fig. 6 shows the evolution of the sorption isotherms after chemical degradation as well as
469 their decomposition into the three mechanisms. The fitting parameters and the experimental
470 data are listed in Appendix (Tables A.3-A.4). The water content decreases slightly after
471 degradation in both cases: for XL membrane, this evolution can be attributed to a decrease of
472 the Langmuir component as well as a reduced Henry's slope (7.2 *vs.* 7.8 for the pristine XL
473 membrane). This water-uptake is nevertheless compensated by a better aggregation of water
474 molecules at high water activity. In the case of the NR211 membrane, similar trends are
475 observed at low and intermediate water activities, with a decrease of the Henry's slope from
476 9.6 to 8.8, but no significant increase at high water activities.

477 *3.3.2 Water self-diffusion coefficient after chemical degradation*

478 The water diffusion coefficient in PFSA membranes is commonly measured thanks to Pulsed-
479 Field Gradient (PFG) NMR experiments. Before detailing these results, it is worth noting that
480 our previous study has shown that the ^{1}H-NMR spectra of both pristine and aged membranes

exhibit two resonance peaks corresponding to two different water populations, *i.e.* water molecules with different chemical environments [41]. These two water populations have also been observed in the present study for both pristine and degraded membranes, whether reinforced or not. One of the two resonance peaks is very intense and well resolved while the other has a very low intensity and can be largely overlapped with the main peak in certain hydration conditions. This makes it difficult to follow the evolution of the small resonance peak. For this reason, only the water self-diffusion coefficient of the most intense peak is considered thereafter.

Fig. 7 shows the evolution of the diffusion coefficient as a function of the water uptake for the pristine and degraded membranes. The experimental values are listed in Table A.5 of Appendix. Firstly, there is a noticeable dispersion in the case of pristine membranes, which may highlight a consequential heterogeneity in pristine state. Furthermore, water self-diffusion coefficients of pristine XL and NR211 membranes are in agreement with those reported in the literature for first generation Nafion™ membranes [73–75].

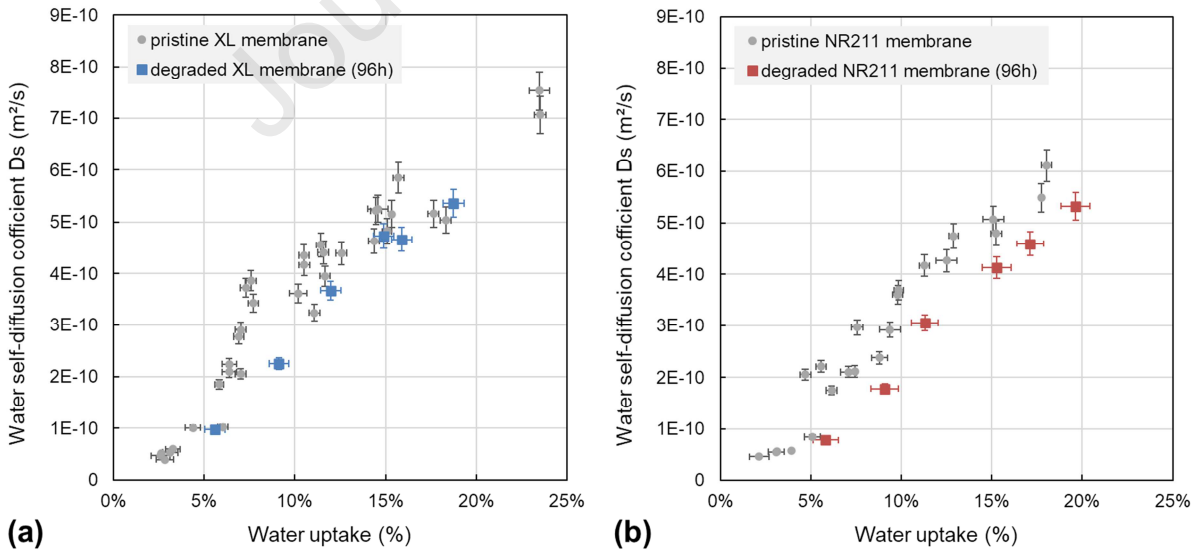

Fig. 7. Water self-diffusion coefficient evolution after 96 hours of Fenton's reagents exposure as a function of water uptake in (a) XL and (b) NR211 membranes (squared symbols) in comparison with pristine membranes (circles).

A 96 hours exposure to Fenton's reagents does not lead to significant modifications of the diffusion coefficient *vs.* water activity plots: in the case of degraded XL, the water self-diffusion coefficient is very close to the lower limit of values obtained for a pristine membrane. However, the water self-diffusion coefficient of degraded NR211 seems slightly lower than in pristine state, regardless of the water uptake.

4. Discussion

4.1 Nafion™ XL membrane chemical degradation

Our multi-techniques investigation demonstrates that both reinforced XL and unreinforced NR211 membranes experience non-negligible chemical decomposition with distinct degradation levels. Several complementary indicators, such as weight loss, fluoride and product A – perfluoro(3-oxapentane)-1-sulfonic-4-carboxylic diacid – emissions provided evidences of effective chemical degradation of membranes as a result of radical attacks. However, FTIR-ATR and solid-state ^{19}F-NMR analyses indicated that neither the chemical structure nor the IEC/IEC$_g$ varied. The PFSA membrane degradation mechanisms proposed in the literature involve either radical attacks on both the main and side chains or polymer decomposition starting from the side chains, propagating along the polymer structure, and possibly resulting into the severing of the main chains [8]. In the first case, the chemical degradation can occur without impacting the structure of the polymer repeating unit and thus, does not entail the evolution of the IR or ^{19}F-NMR spectra, as observed in this work. Furthermore, the PFSA degradation mechanisms result from the attack of hydroxyl ($HO^{\bullet}$) and/or hydrogen ($H^{\bullet}$) radicals on vulnerable sites while Fenton's reaction only generates hydroxyl radicals [8]. In this regard, among the various degradation mechanisms implying the $HO^{\bullet}$ radical attack, the presence of product A in our solutions can only be explained by the unzipping reaction on PFSA backbone propagating up to the junction with a side chain and

thus leading to its entire loss [72,76]. Although it has been demonstrated that chemically stabilized Nafion membranes present a reduced number of reactive end groups, they are nevertheless not completely free of vulnerable sites [12]. Moreover, it has been recently shown that although chemically stabilized Nafion™ membranes had lower fluoride emission rates than conventional ones, large fluorinated molecules were still emitted in equivalent or sometimes higher proportions [69,77]: chemical stabilization decreases the ionomer vulnerability against main chain radical attacks but does not inhibit its chemical decomposition *via* unzipping reaction. Additionally, TFA molecules have also been identified in Fenton solution and they can have two origins:

- *via* the radical attack of hydroxyl radical $HO^{\bullet}$ on the ether bond of PFSA side chain, thus leading to the formation of TFA and $HO\text{-}CF_2\text{-}CF_2\text{-}SO_3H$ molecules according to Chen and Fuller [72],
- or through the decomposition of product A into TFA and $HOOC\text{-}CF_2\text{-}SO_3H$ *via* unzipping mechanism, as suggested by Xie and Hayden [76].

Since we did not observe significant IEC evolution, based on the mechanisms proposed in the literature, the chemical decomposition of PFSA most probably occurred through the unzipping of the polymer backbone, leading to the entire loss of the repeat unit and thus to the formation of product A.

The evolutions of water sorption capacity and water self-diffusion coefficient showed that neither the water-uptake behavior nor the water mobility in XL and NR211 membranes were significantly altered after 96 hours of Fenton's reagents exposure. Although the chemical degradation of XL and NR211 membranes was clearly evidenced, it remained probably quite limited compared to what can occur after several thousand hours of operation in fuel cells: this can explain the moderate impact on membranes functional properties. A direct

comparison with the literature is delicate because of the various operating conditions applied – the H_2O_2 concentration being comprised between 3 and 30 % and that of the Fe^{2+} catalyst between 3 and 6000 ppm –; however, the fluoride emission rates we measured were small but realistic [12,25,26]. Recently, Shi *et al.* studied the mechanical properties of Nafion™ XL and NR212 membranes after exposure to Fenton's reagents [17]. Their fluoride emission rates were larger than ours, with more variations between unreinforced NR212 and reinforced XL membranes. However, the authors performed their experiments in more severe conditions than ours: their Fenton's reagents concentration was of about 22.5 % for H_2O_2 and 14 ppm for ferrous ions whereas we have only 3 vol.% of H_2O_2 and 1 ppm of Fe^{2+}. Indeed, it has been recently demonstrated that the fluoride emission rate depends highly on Fenton's reagents concentration [46,47], with systematically lower emission for reinforced XL membranes than their unreinforced counterparts. Moreover, it has been shown that the use of high hydrogen peroxide concentration conducts to severe morphological changes which are – most probably – not representative of fuel cell operating conditions [46,47]. Therefore, in the present work, the moderate concentrations of Fenton's reagents chosen are believed to better replicate the chemical degradation occurring during fuel cell operation.

4.2 Contribution of reinforcement layer and radical scavengers against chemical degradation

The liquid-state ^{19}F-NMR analysis demonstrated that the chemical degradation mechanisms are similar for XL and NR211 membranes and that the emissions of degradation products are slightly lower for reinforced XL than unreinforced NR211 membrane all along the degradation process. When plotted as a function of the exposure time, the cumulative emissions of product A and fluoride ions increase quite linearly, showing rather constant emission rates (Fig. 8).

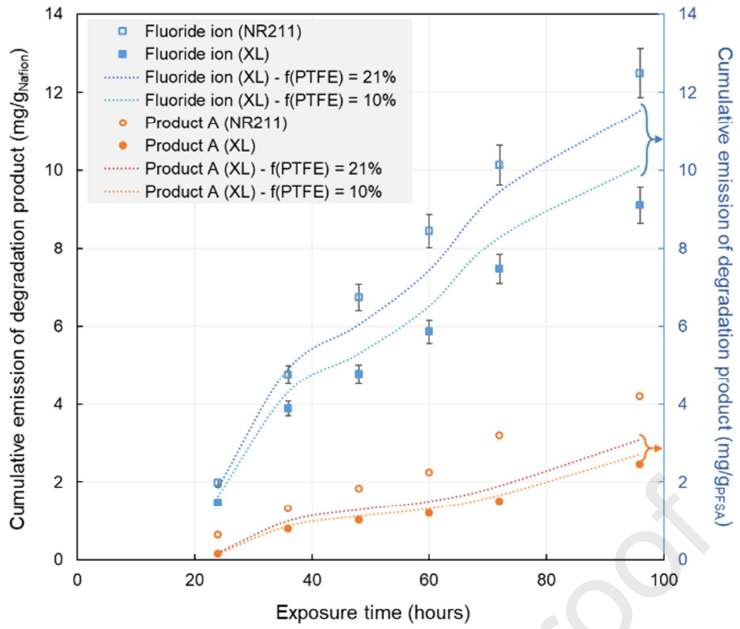

Fig. 8 – Cumulative emissions of degradation products *vs.* exposure time for XL and NR211 membranes. Fluoride emissions (square symbols) were evaluated thanks to the ion-selective electrode while the emissions of Product A (circles) were estimated by quantitative NMR experiments. TFA emissions were not represented here due to their low concentrations. Dotted lines refer to the secondary vertical axis and designate lower/upper boundaries of fluoride emission when PTFE-layer fraction in XL membrane is considered.

However, emissions of degradation products are expressed here in terms of Nafion dry weight and the presence of a reinforcement layer in XL membrane is thus not considered. PTFE being believed to have a greater chemical resistance against radical attacks than PFSA, it could be argued that fluoride emissions only result from the degradation of the PFSA ionomer. PTFE is indeed a hydrophobic non-polar material and has consequently a poor affinity with the aqueous Fenton solution. Moreover, PTFE containing only -CF_2 groups, it cannot release product A. Consequently, the fraction of PTFE-layer must be considered in order to properly compare the emissions of degradation products of XL and NR211 membranes. Thanks to wide-angle X-ray scattering (WAXS) measurements, the PTFE fraction in pristine XL membrane has been evaluated around 21 % [21,34]. On the other hand, Shi *et al.* [34] stated that Nafion XL membrane should contain 10 % of PTFE, 75 % to 90 % of PFSA/TFE copolymer and up to 5 % of proprietary additive compounds. Considering those two values as maximum and minimum limits, the lower and upper boundaries of the actual

amount of degradation products emitted per gram of PFSA can be calculated and plotted in Fig. 8. When expressed in mg/g_{PFSA}, we can observe that the emission of product A is consistently lower with XL membranes, indicating a lower degradation rate than its unreinforced counterpart. The same trend can be observed with fluorine emission, although the difference between XL and NR211 membranes is slightly less pronounced. Considering the evolution of the emissions of fluorine and product A, the PFSA in reinforced XL membrane seems more chemically stable than in NR211 membrane. The better chemical durability of XL membrane could be mainly assigned to the presence of cerium-based radical scavengers into the membrane since, to the best of our knowledge, no publication or commercial information have mentioned the presence of radical scavengers in NR211 membranes. The work of D'Urso *et al.* indeed permitted to demonstrate that the introduction of cerium-based radical scavengers significantly restricts the radicals' concentration and thus the chemical degradation [78]. The authors indeed showed that the introduction of SiO_2 supported cerium-based radical scavengers into reinforced Aquivion® membranes permitted to decrease by around 40 % the fluoride emission rate comparatively to a membrane free of radical scavenger. Additionally, Shi *et al.* recently reported fluoride emission rates more than three times higher for unreinforced NR212 than composite XL membranes and suggested that this discrepancy could be ascribed by the addition of radical scavengers [17]. On the other hand, it cannot be excluded that the PTFE reinforcement layer could also play a role in limiting the chemical degradation. Better mechanical properties of composite membranes have indeed been proven [35,37,38] and could explain, at least partially, the reinforcement contribution in protecting or slowing down the PFSA degradation by ensuring a better membrane integrity and thus preventing further chemical decomposition. However, it is not possible at this point to clearly conclude about the contribution of each mitigation strategy on the chemical stability of XL membranes.

Finally, we recently studied the chemical degradation of reinforced PFSA membranes after 12860 hours [42] of fuel cell operation. The significant intensity decrease of C–O–C and S–O stretching bands detected by FTIR-ATR spectroscopy indicated a partial loss of the PFSA side chains as well as a significant IEC reduction. Additionally, a decrease of water sorption capacity as well as a reduced water mobility have been observed and it has been suggested that this trend could be partly due to the partial loss of sulfonic groups by side chain cleavages. Such results are clearly different from those reported here following *ex-situ* chemical stress tests, since neither chemical structure evolution nor significant change of water uptake and water diffusion was observed. This may indicate that the polymer decomposition caused by radical attacks during short duration (i.e. 96 *vs.* > 12000 hours) – even though the Fenton process employed here is supposed to mimic an accelerated degradation – is not fully representative of the impact of membrane degradation on water sorption and transport properties. Degradation occurring during fuel cell operation is indeed believed to occur due to complex and interrelated mechanical and chemical degradation mechanisms. Future studies of the impact of conjoint chemical and mechanical *ex-situ* degradation modes on PFSA membrane structure and properties will probably help to complement our understandings of PFSA degradation mechanisms and aging phenomena.

5. Conclusion

The impact of *ex-situ* chemical degradation induced by Fenton's reaction on the structure and the water sorption and transport properties of composite Nafion™ XL membrane was explored and compared to that of unreinforced Nafion™ NR211 membrane. To the best of our knowledge, recent investigations have been only focused on the impact of chemical degradation or the contribution of reinforcement layer to the mechanical durability of XL membrane, but none of them have studied its chemical stability. This paper aimed at providing some understandings on the chemical degradation of the XL membrane and

clarifying the contribution of the reinforcement layer and radical scavengers on polymer decomposition rate. Our results permitted to highlight the following items:

- Reinforced XL membrane is chemically degraded by Fenton's reagents exposure, even though it contains an additional reinforcement layer and radical scavengers comparatively to its non-reinforced analogue, the NR211 membrane. In addition to important weight loss, fluoride concentration measurements using ion-selective electrode and liquid-state ^{19}F-NMR analysis highlighted significant emissions of fluoride ions and perfluoro(3-oxapentane)-1-sulfonic-4-carboxylic diacid (named product A in the paper for clarity), a fluorinated compound deriving from the PFSA side chains which has been already identified in the literature as one of the main PFSA degradation products. Moreover, the presence of identical degradation products for both membranes throughout the degradation process demonstrates that the degradation mechanisms are identical.
- In spite of significant chemical degradation, FTIR-ATR and solid-state ^{19}F-NMR analyses of degraded membranes highlighted no chemical structure evolution as well as no IEC/IEC_g variation, suggesting that degradation of the PFSA main and side chains takes place in equal proportions. Furthermore, the release of product A by the membranes while the IEC_g/IEC of XL and NR211 do not vary could imply that the polymer decomposition occurs *via* an unzipping reaction and leads to the loss of the side chains. Nevertheless, the water sorption and diffusion in degraded XL and NR211 membranes seems not to be significantly altered by the chemical degradation.
- Comparatively to NR211 membrane, when the emissions of degradation products are expressed in mg/g_{PFSA} to discriminate the presence of PTFE reinforcement layer in XL membrane and thus consider solely PFSA degradation, the composite XL membrane seems more enduring against radical attacks than its non-reinforced analogue. This

difference may be explained by the presence of the additional PTFE layer, which could help to maintain the membrane mechanical integrity and thus avoid further chemical decomposition, and/or by the presence of cerium-based radical scavengers into the XL membrane which can mitigate the radical attacks on the polymer chains.

Acknowledgements

This research was partially funded by the Greater East Region.

Appendix A.

See Tables A.1–A.5.

Table A.1 – Averaged normalized intensity of PFSA side chain bands as a function of exposure time.

		t = 0 h	t = 24 h	t = 36 h	t = 48 h	t = 60 h	t = 72 h	t = 96 h
XL membrane	$\nu_s(COC_{sc})$	0.451 ± 0.002	0.452 ± 0.003	0.460 ± 0.008	0.447 ±0.003	0.449 ± 0.02	0.434 ± 0.009	0.444 ± 0.003
	$\nu_s(COC_{bk})$	0.448 ± 0.001	0.450 ± 0.002	0.455 ± 0.008	0.447 ± 0.002	0.443 ± 0.02	0.442 ± 0.004	0.442 ± 0.006
	$\nu_s(SO_3^-)$	0.579 ± 0.008	0.581 ± 0.006	0.586 ± 0.012	0.570 ± 0.007	0.577 ± 0.005	0.560 ± 0.007	0.568 ± 0.007
NR211 membrane	$\nu_s(COC_{sc})$	0.393 ± 0.001	0.380 ± 0.004	0.380 ± 0.008	0.389 ± 0.003	0.385 ± 0.003	0.370 ± 0.007	0.381 ± 0.004
	$\nu_s(COC_{bk})$	0.393 ± 0.003	0.384 ± 0.004	0.388 ± 0.005	0.387 ± 0.004	0.386 ± 0.004	0.383 ± 0.004	0.385 ± 0.003
	$\nu_s(SO_3^-)$	0.415 ± 0.005	0.404 ± 0.004	0.405 ± 0.006	0.404 ± 0.004	0.408 ± 0.004	0.395 ± 0.007	0.407 ± 0.005

Table A.2 – Cumulative emissions of fluoride ions and product A as a function of exposure time.

		t = 24 h	t = 36 h	t = 48 h	t = 60 h	t = 72h	t = 96 h
XL membrane	Cumulative fluoride emission (mg/g_{Nafion})	1.458 ± 0.073	3.888 ± 0.194	4.775 ± 0.239	5.863 ± 0.293	7.460 ± 0.373	9.103 ± 0.455
	Cumulative product A emission (mg/g_{Nafion})	0.137 ± 0.013	0.782 ± 0.022	1.008 ± 0.053	1.181 ± 0.065	1.498 ± 0.087	2.441 ± 0.114
NR211 membrane	Cumulative fluoride emission (mg/g_{Nafion})	1.971 ± 0.099	4.764 ± 0.238	6.733 ± 0.337	8.443 ± 0.422	10.128 ± 0.506	12.483 ± 0.624
	Cumulative product A	0.625 ±	1.302 ±	1.827 ±	2.238 ±	3.188 ±	4.199 ±

emission (mg/g_{Nafion})	0.035	0.054	0.073	0.123	0.203	0.226

Table A.3 – Water uptake $\frac{\Delta m}{m_{dry}}$ (%) as a function of water activity at 30°C.

Pristine XL membrane		Degraded XL membrane (96h)		Pristine NR211 membrane		Degraded NR211 membrane (96h)	
Water activity	Water uptake	Water activity	Water uptake	Water activity	Water uptake	Water activity	Water uptake
0.01	0.08 ± 0.11	0.01	0.02 ± 0.01	0.01	0.04 ± 0.11	0.01	0.01 ± 0.00
0.05	1.45 ± 0.14	0.05	1.24 ± 0.09	0.05	1.90 ± 0.14	0.05	1.54 ± 0.07
0.10	2.07 ± 0.13	0.10	1.77 ± 0.08	0.10	2.65 ± 0.13	0.10	2.15 ± 0.09
0.15	2.57 ± 0.10	0.15	2.19 ± 0.09	0.15	3.25 ± 0.10	0.15	2.65 ± 0.07
0.20	3.04 ± 0.07	0.20	2.56 ± 0.10	0.20	3.78 ± 0.07	0.20	3.10 ± 0.08
0.25	3.46 ± 0.06	0.25	2.91 ± 0.09	0.25	4.30 ± 0.06	0.25	3.54 ± 0.09
0.30	3.88 ± 0.05	0.30	3.27 ± 0.08	0.30	4.87 ± 0.05	0.30	3.97 ± 0.09
0.35	4.30 ± 0.04	0.35	3.64 ± 0.09	0.35	5.36 ± 0.04	0.35	4.41 ± 0.10
0.40	4.71 ± 0.03	0.40	4.01 ± 0.08	0.40	5.84 ± 0.03	0.40	4.86 ± 0.11
0.45	5.12 ± 0.03	0.45	4.39 ± 0.07	0.45	6.36 ± 0.03	0.45	5.31 ± 0.05
0.50	5.54 ± 0.03	0.50	4.79 ± 0.06	0.50	6.84 ± 0.03	0.50	5.80 ± 0.06
0.55	5.97 ± 0.03	0.55	5.20 ± 0.07	0.55	7.41 ± 0.03	0.55	6.34 ± 0.02
0.60	6.44 ± 0.04	0.60	5.66 ± 0.06	0.60	7.94 ± 0.04	0.60	6.90 ± 0.05
0.65	6.93 ± 0.04	0.65	6.19 ± 0.09	0.65	8.50 ± 0.04	0.65	7.55 ± 0.09
0.70	7.49 ± 0.05	0.70	6.79 ± 0.01	0.70	9.27 ± 0.05	0.70	8.32 ± 0.20
0.75	8.13 ± 0.07	0.75	7.65 ± 0.12	0.75	10.09 ± 0.07	0.75	9.13 ± 0.19
0.80	8.89 ± 0.10	0.80	8.45 ± 0.08	0.80	11.02 ± 0.10	0.80	10.20 ± 0.09
0.85	9.79 ± 0.13	0.85	9.46 ± 0.03	0.85	12.34 ± 0.13	0.85	11.38 ± 0.01
0.90	10.96 ± 0.20	0.90	10.83 ± 0.03	0.90	13.90 ± 0.20	0.90	12.93 ± 0.10
0.95	12.65 ± 0.32	0.95	12.66 ± 0.10	0.95	16.22 ± 0.32	0.95	15.33 ± 0.34

Table A.4 – Fitting parameters of water sorption isotherm for $0 < a_{water} < 0.60$.

	Pristine XL membrane	Degraded XL membrane (96h)	Pristine NR211 membrane	Degraded NR211 membrane (96h)
Parameter A	1.81 ± 0.16	1.27 ± 0.11	2.25 ± 0.13	1.50 ± 0.15
Parameter B	21.40 ± 5.03	32.49 ± 9.52	25.65 ± 4.30	29.60 ± 8.50

Parameter C (Henry's slope)	7.80 ± 0.25	7.22 ± 0.19	9.58 ± 0.21	8.49 ± 0.28

680

681 **Table A.5 –** Water self-diffusion coefficient D_s (10^{-10} m².cm^{-1}) as a function of water uptake at 24°C.

Pristine XL membrane		Degraded XL membrane (96h)		Pristine NR211 membrane		Degraded NR211 membrane (96h)	
Water uptake	D_s	Water uptake	D_s	Water uptake	D_s	Water uptake	D_s
2.60 %	0.47	5.59 %	0.97	2.15 %	0.46	5.82 %	0.78
2.65 %	0.52	9.11 %	2.25	3.08 %	0.55	9.09 %	1.79
2.84 %	0.39	11.97 %	3.67	3.15 %	0.56	11.30 %	3.06
3.13 %	0.53	14.89 %	4.73	3.94 %	0.58	15.27 %	4.13
3.29 %	0.59	15.89 %	4.66	4.69 %	2.06	17.12 %	4.60
4.38 %	1.01	18.75 %	5.36	5.09 %	0.84	19.64 %	5.33
5.84 %	1.85			5.57 %	2.21		
6.02 %	1.02			6.16 %	1.75		
6.38 %	2.09			7.08 %	2.10		
6.38 %	2.24			7.43%	2.12		
6.91 %	2.77			7.56%	2.96		
7.01 %	2.90			8.79%	2.37		
7.01 %	2.06			9.38%	2.92		
7.29 %	3.72			9.81%	3.60		
7.57 %	3.86			9.85%	3.69		
7.70 %	3.42			11.27%	4.17		
10.19 %	3.62			12.50%	4.27		
10.49 %	4.35			12.90%	4.75		
10.52 %	4.17			15.09%	5.07		
11.08 %	3.24			15.25%	4.80		
11.44 %	4.56			17.73%	5.49		
11.58 %	4.41			18.04%	6.11		
11.66 %	3.95						
12.57 %	4.40						
14.36 %	4.63						
14.48 %	5.22						

14.58 %	5.26
15.08 %	4.82
15.34 %	5.15
15.71 %	5.85
17.65 %	5.16
18.33 %	5.03
23.48 %	7.53
23.53 %	7.07

References

[1] R. Borup, J. Meyers, B. Pivovar, Y.S. Kim, R. Mukundan, N. Garland, D. Myers, M. Wilson, F. Garzon, D. Wood, P. Zelenay, K. More, K. Stroh, T. Zawodzinski, J. Boncella, J.E. McGrath, M. Inaba, K. Miyatake, M. Hori, K. Ota, Z. Ogumi, S. Miyata, A. Nishikata, Z. Siroma, Y. Uchimoto, K. Yasuda, K. Kimijima, N. Iwashita, Scientific aspects of polymer electrolyte fuel cell durability and degradation, Chem. Rev. 107 (2007) 3904–3951. https://doi.org/10.1021/cr050182l.

[2] L. Dubau, L. Castanheira, F. Maillard, M. Chatenet, O. Lottin, G. Maranzana, J. Dillet, A. Lamibrac, J.-C. Perrin, E. Moukheiber, A. ElKaddouri, G. De Moor, C. Bas, L. Flandin, N. Caque, A review of PEM fuel cell durability: materials degradation, local heterogeneities of aging and possible mitigation strategies, Wiley Interdiscip. Rev.-Energy Environ. 3 (2014) 540–560. https://doi.org/10.1002/wene.113.

[3] J. Zhao, X. Li, A review of polymer electrolyte membrane fuel cell durability for vehicular applications: Degradation modes and experimental techniques, Energy Convers. Manag. 199 (2019) 112022. https://doi.org/10.1016/j.enconman.2019.112022.

[4] A. Kusoglu, A.Z. Weber, New Insights into Perfluorinated Sulfonic-Acid Ionomers, Chem. Rev. 117 (2017) 987–1104. https://doi.org/10.1021/acs.chemrev.6b00159.

[5] A. Kusoglu, A.Z. Weber, Electrochemical/Mechanical Coupling in Ion-Conducting Soft Matter, J. Phys. Chem. Lett. 6 (2015) 4547–4552. https://doi.org/10.1021/acs.jpclett.5b01639.

[6] M.P. Rodgers, L.J. Bonville, H.R. Kunz, D.K. Slattery, J.M. Fenton, Fuel Cell Perfluorinated Sulfonic Acid Membrane Degradation Correlating Accelerated Stress Testing and Lifetime, Chem. Rev. 112 (2012) 6075–6103. https://doi.org/10.1021/cr200424d.

[7] A.B. LaConti, M. Hamdan, R.C. McDonald, Mechanisms of membrane degradation, in: Handb. Fuel Cells, John Wiley & Sons, Ltd, 2003. https://doi.org/10.1002/9780470974001.f303055.

[8] M. Zatoń, J. Rozière, D.J. Jones, Current understanding of chemical degradation mechanisms of perfluorosulfonic acid membranes and their mitigation strategies: a review, Sustain. Energy Fuels. 1 (2017) 409–438. https://doi.org/10.1039/C7SE00038C.

[9] M. Danilczuk, F.D. Coms, S. Schlick, Visualizing Chemical Reactions and Crossover Processes in a Fuel Cell Inserted in the ESR Resonator: Detection by Spin Trapping of Oxygen Radicals, Nafion-Derived Fragments, and Hydrogen and Deuterium Atoms, J. Phys. Chem. B. 113 (2009) 8031–8042. https://doi.org/10.1021/jp901597f.

[10] S.-Y. Lee, E. Cho, J.-H. Lee, H.-J. Kim, T.-H. Lim, I.-H. Oh, J. Won, Effects of purging on the degradation of PEMFCs operating with repetitive on/off cycles, J. Electrochem. Soc. 154 (2007) B194–B200. https://doi.org/10.1149/1.2403083.
[11] J. Healy, C. Hayden, T. Xie, K. Olson, R. Waldo, A. Brundage, H. Gasteiger, J. Abbott, Aspects of the chemical degradation of PFSA ionomers used in PEM fuel cells, Fuel Cells. 5 (2005) 302–308. https://doi.org/10.1002/fuce.200400050.
[12] D.E. Curtin, R.D. Lousenberg, T.J. Henry, P.C. Tangeman, M.E. Tisack, Advanced materials for improved PEMFC performance and life, J. Power Sources. 131 (2004) 41–48. https://doi.org/10.1016/j.jpowsour.2004.01.023.
[13] I. Nitta, S. Karvonen, O. Himanen, M. Mikkola, Modelling the Effect of Inhomogeneous Compression of GDL on Local Transport Phenomena in a PEM Fuel Cell, Fuel Cells. 8 (2008) 410–421. https://doi.org/10.1002/fuce.200700058.
[14] A. Kusoglu, A.Z. Weber, A Mechanistic Model for Pinhole Growth in Fuel-Cell Membranes during Cyclic Loads, J. Electrochem. Soc. 161 (2014) E3311–E3322. https://doi.org/10.1149/2.036408jes.
[15] C.S. Gittleman, F.D. Coms, Y.-H. Lai, Chapter 2 - Membrane Durability: Physical and Chemical Degradation, in: M.M. Mench, E.C. Kumbur, T.N. Veziroglu (Eds.), Polym. Electrolyte Fuel Cell Degrad., Academic Press, Boston, 2012: pp. 15–88. https://doi.org/10.1016/B978-0-12-386936-4.10002-8.
[16] G.D. Moor, C. Bas, N. Charvin, E. Moukheiber, F. Niepceron, N. Breilly, J. André, E. Rossinot, E. Claude, N.D. Albérola, L. Flandin, Understanding Membrane Failure in PEMFC: Comparison of Diagnostic Tools at Different Observation Scales, Fuel Cells. 12 (2012) 356–364. https://doi.org/10.1002/fuce.201100161.
[17] S. Shi, X. Sun, Q. Lin, J. Chen, Y. Fu, X. Hong, C. Li, X. Guo, G. Chen, X. Chen, Fatigue crack propagation behavior of fuel cell membranes after chemical degradation, Int. J. Hydrog. Energy. (2020) S0360319920326884. https://doi.org/10.1016/j.ijhydene.2020.07.113.
[18] W. Yoon, X. Huang, Acceleration of Chemical Degradation of Perfluorosulfonic Acid Ionomer Membrane by Mechanical Stress: Experimental Evidence, ECS Trans. 33 (2010) 907–911. https://doi.org/10.1149/1.3484584.
[19] A. Kusoglu, M. Calabrese, A.Z. Weber, Effect of Mechanical Compression on Chemical Degradation of Nafion Membranes, ECS Electrochem. Lett. 3 (2014) F33–F36. https://doi.org/10.1149/2.008405eel.
[20] C. Lim, L. Ghassemzadeh, F. Van Hove, M. Lauritzen, J. Kolodziej, G.G. Wang, S. Holdcroft, E. Kjeang, Membrane degradation during combined chemical and mechanical accelerated stress testing of polymer electrolyte fuel cells, J. Power Sources. 257 (2014) 102–110. https://doi.org/10.1016/j.jpowsour.2014.01.106.
[21] R. Mukundan, A.M. Baker, A. Kusoglu, P. Beattie, S. Knights, A.Z. Weber, R.L. Borup, Membrane Accelerated Stress Test Development for Polymer Electrolyte Fuel Cell Durability Validated Using Field and Drive Cycle Testing, J. Electrochem. Soc. 165 (2018) F3085–F3093. https://doi.org/10.1149/2.0101806jes.
[22] S. Zhang, X. Yuan, H. Wang, W. Mérida, H. Zhu, J. Shen, S. Wu, J. Zhang, A review of accelerated stress tests of MEA durability in PEM fuel cells, Int. J. Hydrog. Energy. 34 (2009) 388–404. https://doi.org/10.1016/j.ijhydene.2008.10.012.
[23] M.P. Rodgers, L.J. Bonville, R. Mukundan, R.L. Borup, R. Ahluwalia, P. Beattie, R.P. Brooker, N. Mohajeri, H.R. Kunz, D.K. Slattery, J.M. Fenton, Perfluorinated Sulfonic Acid Membrane and Membrane Electrode Assembly Degradation Correlating Accelerated Stress Testing and Lifetime Testing, ECS Trans. 58 (2013) 129–148. https://doi.org/10.1149/05801.0129ecst.

766 [24] H. Tang, S. Peikang, S.P. Jiang, F. Wang, M. Pan, A degradation study of Nafion proton
767 exchange membrane of PEM fuel cells, J. Power Sources. 170 (2007) 85–92.
768 https://doi.org/10.1016/j.jpowsour.2007.03.061.
769 [25] S. Kundu, L.C. Simon, M.W. Fowler, Comparison of two accelerated Nafion™
770 degradation experiments, Polym. Degrad. Stab. 93 (2008) 214–224.
771 https://doi.org/10.1016/j.polymdegradstab.2007.10.001.
772 [26] L. Merlo, A. Ghielmi, L. Cirillo, M. Gebert, V. Arcella, Resistance to peroxide
773 degradation of Hyflon® Ion membranes, J. Power Sources. 171 (2007) 140–147.
774 https://doi.org/10.1016/j.jpowsour.2006.11.012.
775 [27] S. Mu, C. Xu, Q. Yuan, Y. Gao, F. Xu, P. Zhao, Degradation behaviors of
776 perfluorosulfonic acid polymer electrolyte membranes for polymer electrolyte
777 membrane fuel cells under varied acceleration conditions, J. Appl. Polym. Sci. 129
778 (2013) 1586–1592. https://doi.org/10.1002/app.38785.
779 [28] L. Ghassemzadeh, K.D. Kreuer, J. Maier, K. Mueller, Evaluating chemical degradation
780 of proton conducting perfluorosulfonic acid ionomers in a Fenton test by solid-state F-19
781 NMR spectroscopy, J. Power Sources. 196 (2011) 2490–2497.
782 https://doi.org/10.1016/j.jpowsour.2010.11.053.
783 [29] T. Kinumoto, M. Inaba, Y. Nakayama, K. Ogata, R. Umebayashi, A. Tasaka, Y. Iriyama,
784 T. Abe, Z. Ogumi, Durability of perfluorinated ionomer membrane against hydrogen
785 peroxide, J. Power Sources. 158 (2006) 1222–1228.
786 https://doi.org/10.1016/j.jpowsour.2005.10.043.
787 [30] K. Hongsirikarn, X. Mo, J.G. Goodwin, S. Creager, Effect of H2O2 on Nafion®
788 properties and conductivity at fuel cell conditions, J. Power Sources. 196 (2011) 3060–
789 3072. https://doi.org/10.1016/j.jpowsour.2010.11.133.
790 [31] X. Luo, L. Ghassemzadeh, S. Holdcroft, Effect of free radical-induced degradation on
791 water permeation through PFSA ionomer membranes, Int. J. Hydrog. Energy. 40 (2015)
792 16714–16723. https://doi.org/10.1016/j.ijhydene.2015.07.118.
793 [32] F. Wang, H. Tang, M. Pan, D. Li, Ex situ investigation of the proton exchange
794 membrane chemical decomposition, Int. J. Hydrog. Energy. 33 (2008) 2283–2288.
795 https://doi.org/10.1016/j.ijhydene.2008.01.052.
796 [33] A.C. Fernandes, E.A. Ticianelli, A performance and degradation study of Nafion 212
797 membrane for proton exchange membrane fuel cells, J. Power Sources. 193 (2009) 547–
798 554. https://doi.org/10.1016/j.jpowsour.2009.04.038.
799 [34] S. Shi, A.Z. Weber, A. Kusoglu, Structure/property relationship of Nafion XL composite
800 membranes, J. Membr. Sci. 516 (2016) 123–134.
801 https://doi.org/10.1016/j.memsci.2016.06.004.
802 [35] E. Moukheiber, C. Bas, L. Flandin, Understanding the formation of pinholes in PFSA
803 membranes with the essential work of fracture (EWF), Int. J. Hydrog. Energy. 39 (2014)
804 2717–2723. https://doi.org/10.1016/j.ijhydene.2013.03.031.
805 [36] N.S. Khattra, Z. Lu, A.M. Karlsson, M.H. Santare, F.C. Busby, T. Schmiedel, Time-
806 dependent mechanical response of a composite PFSA membrane, J. Power Sources. 228
807 (2013) 256–269. https://doi.org/10.1016/j.jpowsour.2012.11.116.
808 [37] Y. Tang, A. Kusoglu, A.M. Karlsson, M.H. Santare, S. Cleghorn, W.B. Johnson,
809 Mechanical properties of a reinforced composite polymer electrolyte membrane and its
810 simulated performance in PEM fuel cells, J. Power Sources. 175 (2008) 817–825.
811 https://doi.org/10.1016/j.jpowsour.2007.09.093.
812 [38] S.M. Stewart, D. Spernjak, R. Borup, A. Datye, F. Garzon, Cerium Migration through
813 Hydrogen Fuel Cells during Accelerated Stress Testing, Ecs Electrochem. Lett. 3 (2014)
814 F19–F22. https://doi.org/10.1149/2.008404eel.

[39] A.M. Baker, R. Mukundan, D. Spernjak, E.J. Judge, S.G. Advani, A.K. Prasad, R.L. Borup, Cerium Migration during PEM Fuel Cell Accelerated Stress Testing, J. Electrochem. Soc. 163 (2016) F1023–F1031. https://doi.org/10.1149/2.0181609jes.
[40] M. Zatoń, B. Prélot, N. Donzel, J. Rozière, D.J. Jones, Migration of Ce and Mn Ions in PEMFC and Its Impact on PFSA Membrane Degradation, J. Electrochem. Soc. 165 (2018) F3281–F3289. https://doi.org/10.1149/2.0311806jes.
[41] M. Robert, A. El Kaddouri, J.-C. Perrin, S. Leclerc, O. Lottin, Towards a NMR-Based Method for Characterizing the Degradation of Nafion XL Membranes for PEMFC, J. Electrochem. Soc. 165 (2018) F3209–F3216. https://doi.org/10.1149/2.0231806jes.
[42] Q. Lin, X. Sun, X. Chen, S. Shi, Effect of Pretreatment on Microstructure and Mechanical Properties of Nafion™ XL Composite Membrane, Fuel Cells. 19 (2019) 530–538. https://doi.org/10.1002/fuce.201900064.
[43] W. Grot, 9 - Experimental Methods, in: Fluorinated Ionomers Second Ed., William Andrew Publishing, 2011: pp. 211–233. https://doi.org/10.1016/B978-1-4377-4457-6.10009-3.
[44] F. Xu, C. Innocent, B. Bonnet, D.J. Jones, J. Roziere, Chemical modification of perfluorosulfonated membranes with pyrrole for fuel cell application: Preparation, characterisation and methanol transport, Fuel Cells. 5 (2005) 398–405. https://doi.org/10.1002/fuce.200400077.
[45] H.J.H. Fenton, LXXIII.—Oxidation of tartaric acid in presence of iron, J. Chem. Soc. Trans. 65 (1894) 899–910. https://doi.org/10.1039/CT8946500899.
[46] S.H. Frensch, G. Serre, F. Fouda-Onana, H.C. Jensen, M.L. Christensen, S.S. Araya, S.K. Kær, Impact of iron and hydrogen peroxide on membrane degradation for polymer electrolyte membrane water electrolysis: Computational and experimental investigation on fluoride emission, J. Power Sources. 420 (2019) 54–62. https://doi.org/10.1016/j.jpowsour.2019.02.076.
[47] M. Robert, A. El Kaddouri, J.-C. Perrin, K. Mozet, M. Daoudi, J. Dillet, J.-Y. Morel, S. André, O. Lottin, Effects of conjoint mechanical and chemical stress on perfluorosulfonic-acid membranes for fuel cells, J. Power Sources. 476 (2020) 228662. https://doi.org/10.1016/j.jpowsour.2020.228662.
[48] C. Korzeniewski, D.E. Snow, R. Basnayake, Transmission infrared spectroscopy as a probe of Nafion film structure: analysis of spectral regions fundamental to understanding hydration effects, Appl. Spectrosc. 60 (2006) 599–604. https://doi.org/10.1366/000370206777670620.
[49] M. Ludvigsson, J. Lindgren, J. Tegenfeldt, FTIR study of water in cast Nafion films, Electrochimica Acta. 45 (2000) 2267–2271. https://doi.org/10.1016/S0013-4686(99)00438-7.
[50] A.E. Kaddouri, L. Perrin, B. Jean, L. Flandin, C. Bas, Investigation of perfluorosulfonic acid ionomer solutions by 19f NMR and DLS: Establishment of an accurate quantification protocol, J. Polym. Sci. Part B Polym. Phys. 54 (2016) 2210–2222. https://doi.org/10.1002/polb.24130.
[51] T. Yuan, H. Zhang, Z. Zou, S. Khatun, D. Akins, Y. Adam, S. Suarez, A Study of the Effect of Heat-Treatment on the Morphology of Nafion Ionomer Dispersion for Use in the Passive Direct Methanol Fuel Cell (DMFC), Membranes. 2 (2012) 841–854. https://doi.org/10.3390/membranes2040841.
[52] E.O. Stejskal, J.E. Tanner, Spin Diffusion Measurements: Spin Echoes in the Presence of a Time□Dependent Field Gradient, J. Chem. Phys. 42 (1965) 288–292. https://doi.org/10.1063/1.1695690.
[53] L. Yan, Y. Hu, X. Zhang, B. Yue, Chapter Three - Applications of NMR Techniques in the Development and Operation of Proton Exchange Membrane Fuel Cells, in: G.A.

Webb (Ed.), Annu. Rep. NMR Spectrosc., Academic Press, 2016: pp. 149–213. https://doi.org/10.1016/bs.arnmr.2015.11.003.
[54] K.A. Mauritz, R.B. Moore, State of Understanding of Nafion, Chem. Rev. 104 (2004) 4535–4586. https://doi.org/10.1021/cr0207123.
[55] Z. Liang, W. Chen, J. Liu, S. Wang, Z. Zhou, W. Li, G. Sun, Q. Xin, FT-IR study of the microstructure of Nafion® membrane, J. Membr. Sci. 233 (2004) 39–44. https://doi.org/10.1016/j.memsci.2003.12.008.
[56] M. Laporta, M. Pegoraro, L. Zanderighi, Perfluorosulfonated membrane (Nafion): FT-IR study of the state of water with increasing humidity, Phys. Chem. Chem. Phys. 1 (1999) 4619–4628. https://doi.org/10.1039/A904460D.
[57] K.M. Cable, K.A. Mauritz, R.B. Moore, Effects of hydrophilic and hydrophobic counterions on the Coulombic interactions in perfluorosulfonate ionomers, J. Polym. Sci. Part B Polym. Phys. 33 (1995) 1065–1072. https://doi.org/10.1002/polb.1995.090330710.
[58] E. Moukheiber, G. De Moor, L. Flandin, C. Bas, Investigation of ionomer structure through its dependence on ion exchange capacity (IEC), J. Membr. Sci. 389 (2012) 294–304. https://doi.org/10.1016/j.memsci.2011.10.041.
[59] C. Bas, L. Flandin, A.-S. Danero, E. Claude, E. Rossinot, N.D. Alberola, Changes in the Chemical Structure and Properties of a Perfluorosulfonated Acid Membrane Induced by Fuel-Cell Operation, J. Appl. Polym. Sci. 117 (2010) 2121–2132. https://doi.org/10.1002/app.31386.
[60] S. Schlick, G. Gebel, M. Pineri, F. Volino, Fluorine-19 NMR spectroscopy of acid Nafion membranes and solutions, Macromolecules. 24 (1991) 3517–3521. https://doi.org/10.1021/ma00012a008.
[61] G. Meresi, Y. Wang, A. Bandis, P.T. Inglefield, A.A. Jones, W.-Y. Wen, Morphology of dry and swollen perfluorosulfonate ionomer by fluorine-19 MAS, NMR and xenon-129 NMR, Polymer. 42 (2001) 6153–6160. https://doi.org/10.1016/S0032-3861(01)00053-2.
[62] Q. Chen, K. Schmidt-Rohr, F-19 and C-13 NMR signal assignment and analysis in a perfluorinated ionomer (Nafion) by two-dimensional solid-state NMR, Macromolecules. 37 (2004) 5995–6003. https://doi.org/10.1021/ma049759b.
[63] DuPont Product Information: Nafion NR-211 and NR-212 PFSA membrane, 2008., (n.d.). http://www.fuelcellsetc.com/store/DS/N211-N212-properties.pdf.
[64] D.A. Ellis, J.W. Martin, D.C.G. Muir, S.A. Mabury, Development of an 19F NMR Method for the Analysis of Fluorinated Acids in Environmental Water Samples, Anal. Chem. 72 (2000) 726–731. https://doi.org/10.1021/ac9910280.
[65] E. Pretsch, P. Bühlmann, M. Badertscher, Structure Determination of Organic Compounds: Tables of Spectral Data, 4th ed., Springer-Verlag, Berlin Heidelberg, 2009. https://doi.org/10.1007/978-3-540-93810-1.
[66] K. Schaumburg, C. Deverell, Fluorine-19 nuclear magnetic resonance chemical shift of hydrofluoric acid in normal water and heavy water solutions, J. Am. Chem. Soc. 90 (1968) 2495–2499. https://doi.org/10.1021/ja01012a009.
[67] K. Alzewel, Relaxation-Time Measurements on Fluoride Ions in Aqueous-Solutions, Z. Phys. Chem.-Leipz. 255 (1974) 193–198.
[68] M. Hudlicky, Chemical shifts of fluorine in hydrogen fluoride and fluoride ion, J. Fluor. Chem. 28 (1985) 461–472. https://doi.org/10.1016/S0022-1139(00)81136-7.
[69] M. Takasaki, Y. Nakagawa, Y. Sakiyama, K. Tanabe, K. Ookubo, N. Sato, T. Minamide, H. Nakayama, M. Hori, Degradation Study of Perfluorosulfonic Acid Polymer Electrolytes: Approach from Decomposition Product Analysis, J. Electrochem. Soc. 160 (2013) F413–F416. https://doi.org/10.1149/2.076304jes.

[70] C. Zhou, M.A. Guerra, Z.-M. Qiu, Zawodzinski Thomas A., D.A. Schiraldi, Chemical Durability Studies of Perfluorinated Sulfonic Acid Polymers and Model Compounds under Mimic Fuel Cell Conditions, Macromolecules. 40 (2007) 8695–8707. https://doi.org/10.1021/ma071603z.
[71] A.H. Carlsson, L. Joerissen, Accelerated Degradation of Perfluorinated Sulfonic Acid Membranes, ECS Trans. 25 (2009) 725–732. https://doi.org/10.1149/1.3210624.
[72] C. Chen, T.F. Fuller, The effect of humidity on the degradation of Nafion® membrane, Polym. Degrad. Stab. 94 (2009) 1436–1447. https://doi.org/10.1016/j.polymdegradstab.2009.05.016.
[73] T.A. Zawodzinski, M. Neeman, L.O. Sillerud, S. Gottesfeld, Determination of water diffusion coefficients in perfluorosulfonate ionomeric membranes, J. Phys. Chem. 95 (1991) 6040–6044. https://doi.org/10.1021/j100168a060.
[74] C.A. Edmondson, J.J. Fontanella, S.H. Chung, S.G. Greenbaum, G.E. Wnek, Complex impedance studies of S-SEBS block polymer proton-conducting membranes, Electrochimica Acta. 46 (2001) 1623–1628. https://doi.org/10.1016/S0013-4686(00)00762-3.
[75] S. Ma, Q. Chen, F.H. Jøgensen, P.C. Stein, E.M. Skou, 19F NMR studies of Nafion™ ionomer adsorption on PEMFC catalysts and supporting carbons, Solid State Ion. 178 (2007) 1568–1575. https://doi.org/10.1016/j.ssi.2007.10.007.
[76] T. Xie, C.A. Hayden, A kinetic model for the chemical degradation of perfluorinated sulfonic acid ionomers: Weak end groups versus side chain cleavage, Polymer. 48 (2007) 5497–5506. https://doi.org/10.1016/j.polymer.2007.07.043.
[77] S. Schlick, The Chemistry of Membranes Used in Fuel Cells: Degradation and Stabilization, John Wiley & Sons, 2017.
[78] C. D'Urso, C. Oldani, V. Baglio, L. Merlo, A.S. Aricò, Towards fuel cell membranes with improved lifetime: Aquivion® Perfluorosulfonic Acid membranes containing immobilized radical scavengers, J. Power Sources. 272 (2014) 753–758. https://doi.org/10.1016/j.jpowsour.2014.09.045.

Highlights:

- *Ex-situ* chemical degradation of Nafion™ XL and NR211 membranes is analyzed.
- Degradation products suggest a polymer decomposition by unzipping reaction.
- Chemical degradation has no significant impact on water sorption and diffusion.
- XL membrane is more enduring against radical attack than unreinforced NR211.

Declaration of interests

☒ The authors declare that they have no known competing financial interests or personal relationships that could have appeared to influence the work reported in this paper.

☐The authors declare the following financial interests/personal relationships which may be considered as potential competing interests: